Analytical Biochemistry 567 (2019) 63–71

Contents lists available at ScienceDirect

Analytical Biochemistry

journal homepage: www.elsevier.com/locate/yabio

Fabrication of a low background signal glucose biosensor with 3D network materials as the electrocatalyst

Huiling Tang[a], Dehao Cai[a], Tianyao Ren[a], Ping Xiong[a], Yu Liu[a], Hui Gu[a,*], Guoyue Shi[b]

[a] Key Laboratory of Theoretical Organic Chemistry and Functional Molecule of Ministry of Education, Hunan Provincial Key Laboratory of Controllable Preparation and Functional Application of Fine Polymers, School of Chemistry and Chemical Engineering, Hunan University of Science and Technology, Xiangtan, Hunan, 411201, China
[b] Lab of Biochemical Sensing Technology, School of Chemistry and Molecular Engineering, Shanghai Key Laboratory for Urban Ecological Processes and Eco-Restoration, East China Normal University, 500 Dongchuan Road, Shanghai, 200241, China

ARTICLE INFO

Keywords:
Low background
Glucose biosensor
3D network
Sol-gel

ABSTRACT

Glucose oxidase (GOx) based biosensor is an effective method to determine glucose level. However, the biosensors embedded with high electroactive species suffered from high background signal levels, which leading to relative low sensitivity for glucose sensing. In this work, a novel 3D network materials based glucose biosensor with low background signal was constructed, which demonstrated high sensitivity and selectivity towards glucose assay. Here, the combination of ionic liquid modified graphene sheets (GS-IL) and Au nanorods (Au NRs) acted as high electroactive catalyst, and thiol-containing silica sol-gel served as a nonconductive matrix to self-assembly of GS-IL and Au NRs to form the three-dimensional (3D) network materials. Meanwhile, the doping amount of the sol-gel had significant influences on electrochemical performance of the 3D network materials based biosensor. As a result, optimized 3.75% doping 3D network materials were selected to construct the glucose biosensor, which exhibited low background signal and high sensitivity. This biosensor was successfully applied in monitoring the glucose levels of serum and brain microdialysate samples.

1. Introduction

Glucose, one of the most important energy substrate in the brain, plays a crucial role in wide spread disease of the peripheral and central nervous systems as well as cardiovascular disease, nephropathy, retinopathy [1,2]. Therefore, there are continuous interests to develop technically insights into glucose's level involved in biosystem.

GOx based electrochemical biosensors have been extensively exploited in the past year, owing to their low-cost, high sensitivity and potential for real time and in situ detection [3–6]. Other than GOx as the specific recognition unit, an excellent biosensor also embeds highly electroactive species as the electron transfer unit. As is to all, Au nanoparticles is very common in molecular sensing applications, while other gold nanocrystals such as Au NRs have been less well-explored especially its electroactivity in spite of the fact that they have several advantageous features over the spherical gold nanoparticles [7,8]. Yet using single gold nanocrystals as biosensors is problematic because of their inconsistent signal amplification [9]. The discovery of GS in 2004, added a new dimension to electrochemical biosensor research due to the high conductivity, large surface area, good biocompatibility and high electron transfer rate of GS [10–12]. Moreover, it has been verified that the use of GS can avoid the problems associated with single gold nanocrystals [13]. Numerous reports have demonstrated that the biosensors based on GS/Au hybrids are highly electroactive within an electrochemical potential window [14,15]. Although these biosensor exhibited strong voltammetric response, their background signal levels are easily affected by electroactive interfering species, leading to relative low signal-noise ratios [16]. Therefore, nonconductive material such as chitosan, polyethyleneimine and cyclodextrin were commonly doped into GS/Au hybrids to reduce its background signal, thus contributing to glucose biosensors with higher signal-noise ratios [17–20].

Sol-gel with tunable porosity, high thermal stability, chemical inertness, is another alternative matrix, attracting particular attention for biosensor fabrication [21]. It can effectively shield electronic turbulence and hence decrease the fluctuation of background current [22]. The three-dimensional (3D) silica sol-gel network, discovered by Dong group [23], not only provides a 3D structure to increase the enzyme and biomolecules loading, but also facilitates the anchoring of gold nanocrystals through Au—S bonds inside of the network [24]. Thus, the 3D silica sol-gel was a good choice to improve the high background signal obtained by GS/Au hybrids.

Herein, we first employed GS-IL/Au NRs nanocomposite to

* Corresponding author.
E-mail address: hgu@hnust.edu.cn (H. Gu).

https://doi.org/10.1016/j.ab.2018.12.012
Received 5 August 2018; Received in revised form 10 December 2018; Accepted 13 December 2018
Available online 17 December 2018

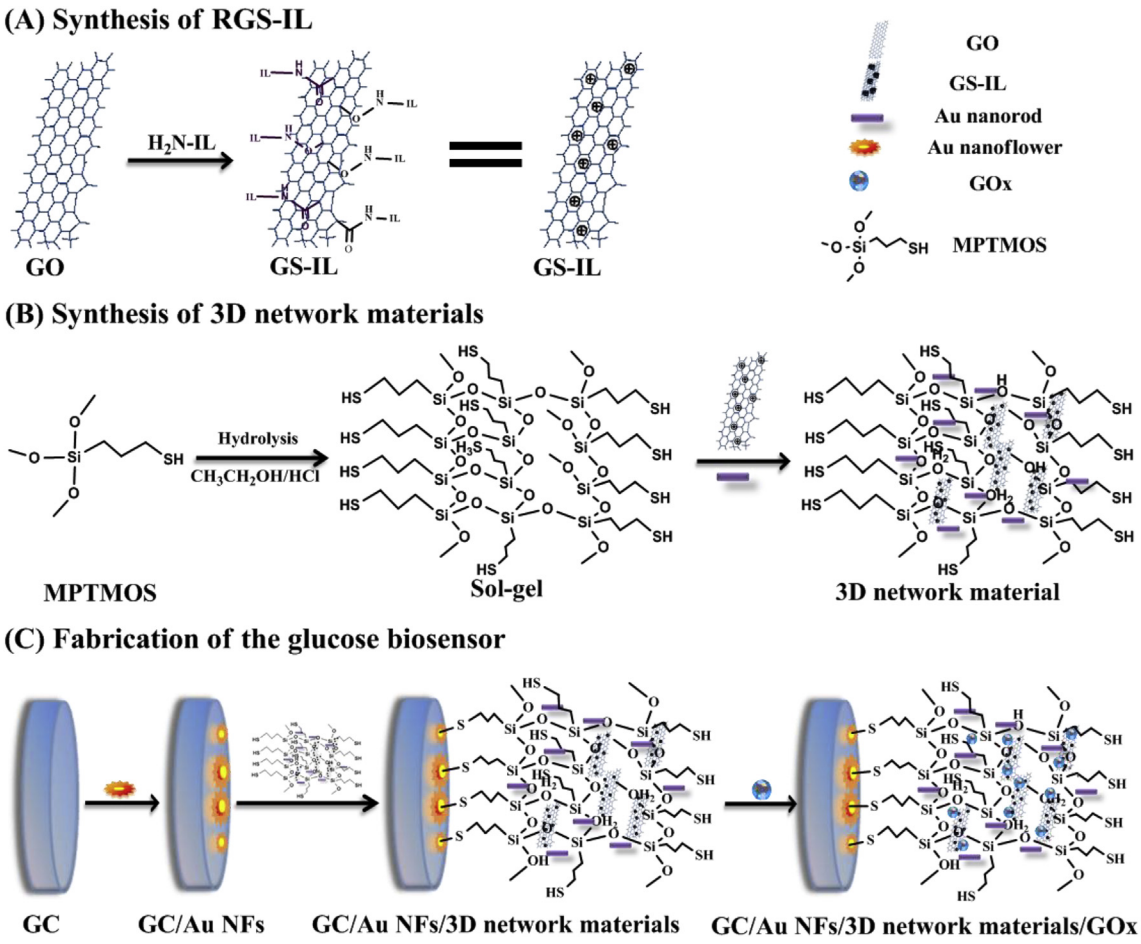

Scheme 1. Schematic illustration of preparing the present glucose biosensor.

construct glucose biosensor, which displayed an ultrahigh background noise. Then the silica sol–gel was used to self-assembly of GS-IL/Au NRs, forming the 3D network materials. With the increasing doping percentage of the sol-gel, the 3D network materials exhibited decreased background noise and response current. As a result, the 3D network materials with 3.75% sol-gel doping based biosensor is superior in terms of having a much lower background response and better signal-to-background ratio, which exhibited high sensitivity, low detection limit, good selectivity. The novel 3D network materials is a promising matrix to fabricate biosensor with high performance, which was successfully applied in actual glucose samples.

2. Materials and methods

2.1. Materials and reagents

1-Methylimidazole (99%), (3-mercaptopropyl) trimethoxy silane (MPTMOS, 95%), Glucose oxidase type VII (GOx, 136000 units/g, EC 1.1.3.4. from aspergillus niger), nafion (5 wt %), norepinephrine hydrochloride (NE, 97%), epinephrine hydrochloride (E, 98%), 3-methyldopamine hydrochloride (3-MT, 99%) and bovine serum albumin (BSA, 98%) were purchased from Sigma-Aldrich (USA). Flake graphite (Asbury Carbons, 230U Grade, High Carbon Natural Graphite 99^{+}), 5-hydroxytryptamine (5-HT, 99%), uric acid (UA, 99%) and dopamine (DA, 99%) were from Alfa Aesar. All the amino acids including leucine (Leu), threonine (Thr), histidine (His), serine (Ser), glutamate (Glu), glycine (Gly), tyrosine (Tyr), tryptophan (Trp), arginine (Arg), and methionine (Met), hydrogen tetrachloroaurate hydrate, $HAuCl_4{\cdot}4H_2O$ (99.9%), hexadecyltrimethylamm-onium bromide (CTAB, 99%), sodium borohydride (96%), ascorbic acid (AA, 99.7%), $AgNO_3$ (99.8%), H_2O_2 (30%) was purchased from Sinopharm Chemical Reagent Co. Ethyl acetate (99.5), N,N-dimethylformamide (99.5%), glucose and lactate (Lac) were from Shanghai Titan Scientific Co. 2-Bromoethylamine hydro-bromide (98%), sodium citrate (98%), glutaraldehyde (25%) were from Adamas-beta. Serum samples were from healthy volunteers provided by local hospital (Xiangtan Central Hospital). The solutions of metal ions were prepared from their chloride salts with double distilled water. All the reagents were of analytical grade and used without further purification. aCSF was prepared by mixing NaCl (144 mM), KCl (2.7 mM), NaH_2PO_4 (1.75 mM), $MgCl_2$ (1 mM), $NaHCO_3$ (2.5 mM), and $CaCl_2$ (1.75 mM), then the pH value was adjusted to 7.4 with NaOH. All aqueous solutions were prepared with doubly distilled water.

2.2. Apparatus

The morphology of Au NRs, GS were examined using a JEOL 2100F field emission transmission electron microscopy (FE-TEM). UV–vis–NIR absorption spectra of the Au NRs solutions were collected using a Perkin Elmer LAMBDA 1050 spectrophotometer. Raman spectra were obtained on a J-Y T64000 Raman spectrometer with 514.5 nm wavelength incident laser light. The XRD patterns were collected on a Bruker D8 ADVANCE instrument using Cu-Kα radiation. All the electrochemical experiments were performed on CHI 830D electrochemical workstation (Shanghai Chenhua Instruments, China). A conventional three-electrode system (Shanghai Chenhua Instruments, China) for the electrochemical experiments composed of a platinum wire as counter electrode, an Ag/AgCl electrode as reference electrode, and a modified

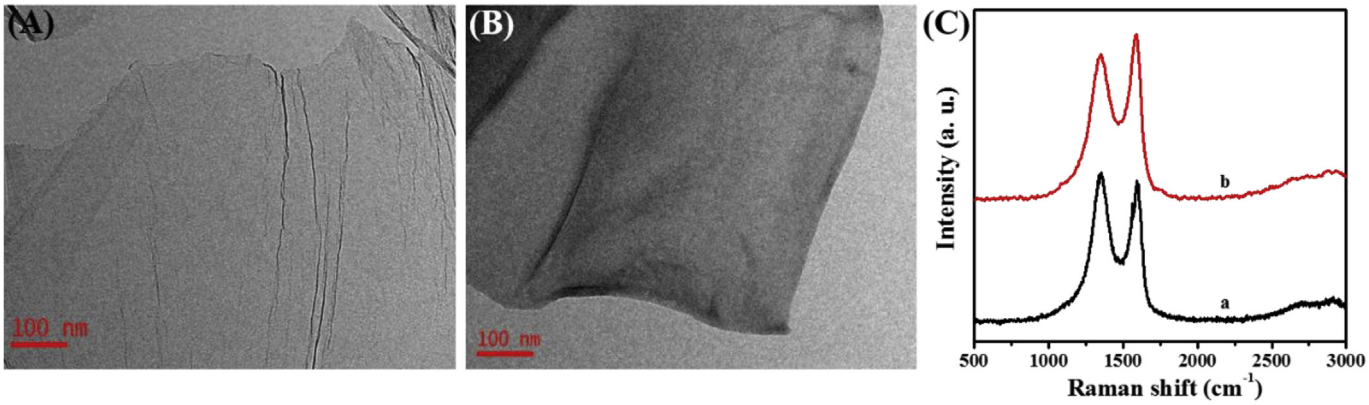

Fig. 1. TEM images of A) GO, B) GS-IL. C) Typical Raman spectra of GO (curve a), GS-IL (curve b).

glassy carbon (GC, 3 mm) electrode as working electrode. All the current-time curve was collected at the potential of −0.2 V. LSV parameters were selected as follows: scan rate of 100 mV/s, sample interval of 1 mV, potential range from 0.4 V or 0.2 V to −0.6 V. In situ monitoring of the dissolution behaviour of Au nanoflowers (Au NFs) during potential cycling in 0.5 M H_2SO_4 was monitored through cyclic voltammograms (CV) measurement. Scan range: −0.5–1.5 V, scan rate: 100 mV/s.

2.3. Fabrication of GC/Au NFs/GS-IL-Au NRs (sol-gel)/GOx biosensor

The fabrication process was depicted in Scheme 1. Firstly, Au NRs with tunable plasmonic peaks were prepared from a modified two-step growth method following the previous literature [25]. Considering co-fabrication of negative charged GOx in 3D network materials, here we employed the positively charged GS-IL which was verified as a promising material for GOx immobilization before [26]. The thiolated aqueous sol-gel was prepared according to the previous literature [23,24]. All of their synthesis procedure was briefly described in ESI. A mixed suspension was prepared by adding sol-gel solution (0 μL, 1 μL, 2 μL, 3 μL, 4 μL, 5.5 μL–11.5 μL) into 40 μL GS-IL and 40 μL Au NRs suspension, which respectively denoted as GS-IL-Au NRs (sol-gel 0%, 1.25%, 2.5%, 3.75%, 5%, 6.25%, 12.5%).

Prior to surface modification, the glassy carbon electrode (GC, 3 mm) was polished with 0.05 μm alumina followed by sonication in HNO_3 (1:1, v/v), NaOH (50%, w/w) and pure distilled water. First, the nanostructured Au NFs were electrochemically deposited on the GC electrode from aqueous solutions of 0.5 M H_2SO_4 containing 20 mM $HAuCl_4$ by applying a potential of −0.2 V for 60 s. The Au NFs electrodeposited electrode was denoted as GC/Au NFs electrode. 5 μL of the above mixed suspension GS-IL-Au NRs (sol-gel 0%, 1.25%, 2.5%, 3.75%, 5%, 6.25%, 12.5%) were casted on the GC/Au NFs electrode respectively, and denoted as GC/Au NFs/GS-IL-Au NRs (sol-gel 0%, 1.25%, 2.5%, 3.75%, 5%, 6.25%, 12.5%) electrodes. After drying and washing thoroughly, 10 μL of GOx solution (10 mg/mL) was incubated on the modified electrodes in a vacuum oven for 30 min. Finally, glutaraldehyde steam was used to trigger the crosslinking reaction and a thin film of 0.5% nafion solution was coated. The resulting GC/Au NFs/GS-IL-Au NRs (sol-gel)/GOx biosensor was stored at 4 °C while not in use.

2.4. Animal experiments and real sample measurements

The experiments involving animals were conducted with the approval of the Animal Ethics Committee in East China Normal University. Male Sprague−Dawley rats (200–300 g) were anesthetized by chloral hydrate (initial dose of 300 mg/kg (i.p.) with additional doses of 50 mg/kg (i.p.) as needed to maintain anaesthesia), and wrapped in a homoeothermic blanket (69000 Series Temperature Controller, WRD Life Science, Shenzhen, China) to keep the body temperature at 37 °C. The rat was placed on a stereotaxic frame (WRD Life Science, Shenzhen, China) with the incisor bar set at 5 mm above the interaural line and appropriately placed holes were drilled through the skull. The microdialysis probe (CMA120, Switzerland) was implanted into the striatum (2.5 mm anterior of bregma, 2.5 mm lateral of midline), and lowered to 7 mm beneath the surface of the brain. In order to reduce the injury of the rat, the microdialysis probe was carefully implanted into the striatum of rats within 30 min. After continuous perfusion for 30 min with aCSF solution, the microdialysis system started to collect microdialysates at a rate of 2.0 μL/min for 3 h as the real sample for glucose determination.

3. Results and discussion

3.1. Characterization of GS-IL, Au NRs

As illustrated in Scheme 1, positively charged GS-IL was used to provide a universal environment for GOx immobilization through electrostatic interactions. First, the size and morphology of GS-IL was investigated by TEM. Graphene oxide (GO) had a typical shape, resembling the large crumpled thin flake (Fig. 1A), and the GS-IL did not change significantly with obvious wrinkles (Fig. 1B). However, the image of the GS-IL was distinguishable from the GO by its appearance of seemly being cover a layer of jelly, which is due to the attachment of IL units to GO. From the Raman spectra (Fig. 1C), the D band (1353 cm^{-1}) and the G band (1595 cm^{-1}) were observed from both GS-IL and GO. The D band corresponds to the defects and the staging disorder in the curved GS, while the G band is related to the sp^2 hybridized carbon. The D/G intensity ratio increased from 0.93 (GO) to 1.07 (GS-IL), which illustrates the GO was reduced at some extent through functionalization [27,28]. The results also indicate the more disorder of the GS-IL than GO, which is because the ionic liquid was attached onto the GO surface through covalent bond [26].

Fig. 2A shows the UV–vis–NIR spectra of the synthesized Au NRs with shifty aspect ratios. Their aspect ratios were various from 2.6, 2.8, 3.1 to 3.4 with the corresponding maximal longitudinal plasmon band wavelengths at 678, 702, 755, and 808 nm, respectively. Increasing the amounts of $AgNO_3$ in the growth solutions resulted in gradual red-shifts of longitudinal peaks, which is basically consistent with the well-known reported method [25]. Fig. 2B exhibits the TEM image of the Au NRs with aspect ratio 2.6 (length: 42 ± 3 nm, width: 16 ± 1.3 nm).

For the biosensor construction, Au NFs were firstly electrochemically deposited onto the electrode, forming a gold platform. The typical SEM image for GC/Au NFs in Fig. S1A revealed that Au NFs were well distributed on the GC electrode like nanostructured flowers with typical size ranging from 600 to 1000 nm. The crystalline

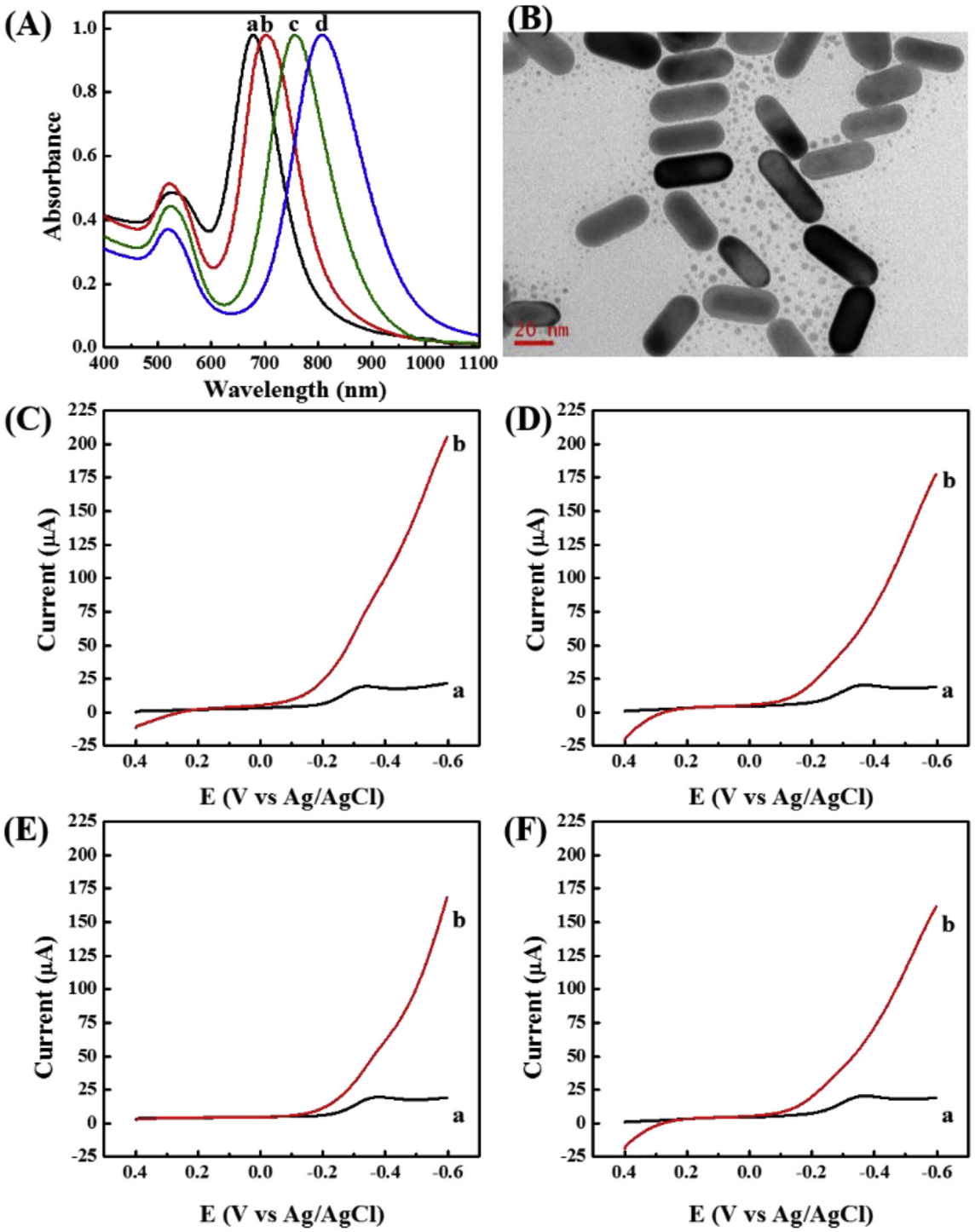

Fig. 2. A) UV–vis–NIR spectra of Au NRs a, b, c, d spectra correspond to aspect ratio 2.6, 2.8, 3.1, and 3.4, respectively. B) TEM images of Au NRs with aspect ratio of 2.6. Note: the splotches among Au NRs are the residual ethanol used to dilute Au NRs. LSV performances of Au NRs correspond to aspect ratio C) 2.6, D) 2.8, E) 3.1, and F) 3.4 modified electrodes in aCSF (a) without, and (b) with 5 mM H_2O_2.

orientation of Au NFs was further characterized by XRD pattern (Fig. S1B). Three typical peaks located at 38.29°, 44.48°, 64.65° were obviously observed, corresponding to (111), (200), (220) facets respectively, which indicates the Au NFs were composed of pure crystalline gold with the face-centered cubic structure [29]. Fig. S2 shows the cyclic voltammogram (CV) of GC/Au NFs electrode in 0.5 M H_2SO_4. A rise in anodic current at 0.57 V indicates oxide formation and reduction of the oxides started at around 0.57 V in the cathodic scan, which is the characteristic CV of Au in acidic solution [30,31].

3.2. Electrochemical behaviour of the 3D network materials toward H_2O_2

To investigate the electrochemical behaviour of the 3D network materials towards H_2O_2, the electrocatalytical activities of the Au NRs towards H_2O_2 were firstly checked. The typical LSV performances of the four Au NRs modified electrodes in aCSF without (curve a) and with (curve b) 5 mM H_2O_2 solution were showed in Fig. 2C, D, E, F. Obvious differences could be seen at four Au NRs modified electrodes with respect to on-set potential and the magnitudes of reduction current.

Obviously, compared other Au NRs, Au NRs (aspect ratio: 2.6) revealed much higher response current and lower on-set potential. As a result, the Au NRs (aspect ratio: 2.6) was used for the following self-assembly of 3D network materials.

Then, effects of the sol-gel doping percentage (sol-gel 0%, 1.25%, 2.5%, 3.75%, 5%, 6.25%, 12.5%) on the electron transfer performance of the 3D network materials were tested (Fig. S3A). A step-by-step enhanced peak-to-peak separations and attenuation process in peak currents were observed on the GC/Au NFs/GS-IL-Au NRs (sol-gel 0%–12.5%) electrodes, which evidences that the electron transfer of $Fe(CN)_6^{3-/4-}$ becomes more and more impeditive with the stepwise increase in sol-gel doping. These results were confirmed by electrochemical impedance measurements in Fig. S3B on the other hand.

Because increase in concentration of glucose is usually measured with the generation of H_2O_2 or the consumption of O_2 [32,33], the electrocatalytic activities of the 3D network materials towards H_2O_2 and O_2 was studied (Fig. S4). Upon addition of H_2O_2, the reduction peak current started to increase significantly at -0.05 V, while removing the O_2 in air caused an obvious decrease in the reduction peak current at -0.2 V. In consideration of the interference from O_2, -0.2 V was selected as the optimal working potential and used in the following electrochemical experiments.

The effects of the sol-gel doping percentage (sol-gel 0%, 1.25%, 2.5%, 3.75%, 5%, 6.25%, 12.5%) on the response sensitivity of the 3D network materials towards H_2O_2 were investigated (Fig. 3A). The amperometric responses of the fabricated electrodes towards the detection of H_2O_2 have been carefully recorded by successively adding 100 μM H_2O_2 in aCSF solution. Large background noise and negligible current response with each addition of 100 μM H_2O_2 were found on the GC/Au NFs/GS-IL-Au NRs (so-gel 0%, curve a) electrode. The loadings of Au NFs with anisotropy and GS-IL-Au NRs increase the electroactive surface area, thus causing the increase in the double-layer capacitance and charge build-up at the double-layer interface. The extremely high noise are probably due to the large electroactive surface area in response to a change in the applied potential at the electrode-electrolyte interface. Therefore, GC/Au NFs/GS-IL-Au NRs (so-gel 0%, curve a) electrode demonstrated poor sensitivity towards H_2O_2. However, gradually descending signal reduction currents and background noises were observed with each GC/Au NFs/GS-IL-Au NRs (sol-gel 1.25%, curve b; 2.5%, curve c; 3.75%, curve d; 5%, curve e; 6.25%, curve f; 12.5%, curve g) electrodes. The specific results were summarized in Fig. 3B. It can be clearly witnessed the signal/noise value increased with increasing doing of sol-gel, which revealed tiny sol-gel addition could dramatically improve the background noise thus promote its signal/noise value. This suggests that 3D network materials assembled from sol-gel has a variety of pore interconnections that may facilitate the transport of the H_2O_2 and electron. However, the signal-to-noise levels declined above 3.75% sol-gel doping, suggesting that excess non-conductive matrix loading starts to place a certain limitation on the H_2O_2 and electron transfer from the small mesopores to electrode surface. As a result, the 3D network materials with 3.75% sol-gel doping modified electrode is superior in terms of having a much lower

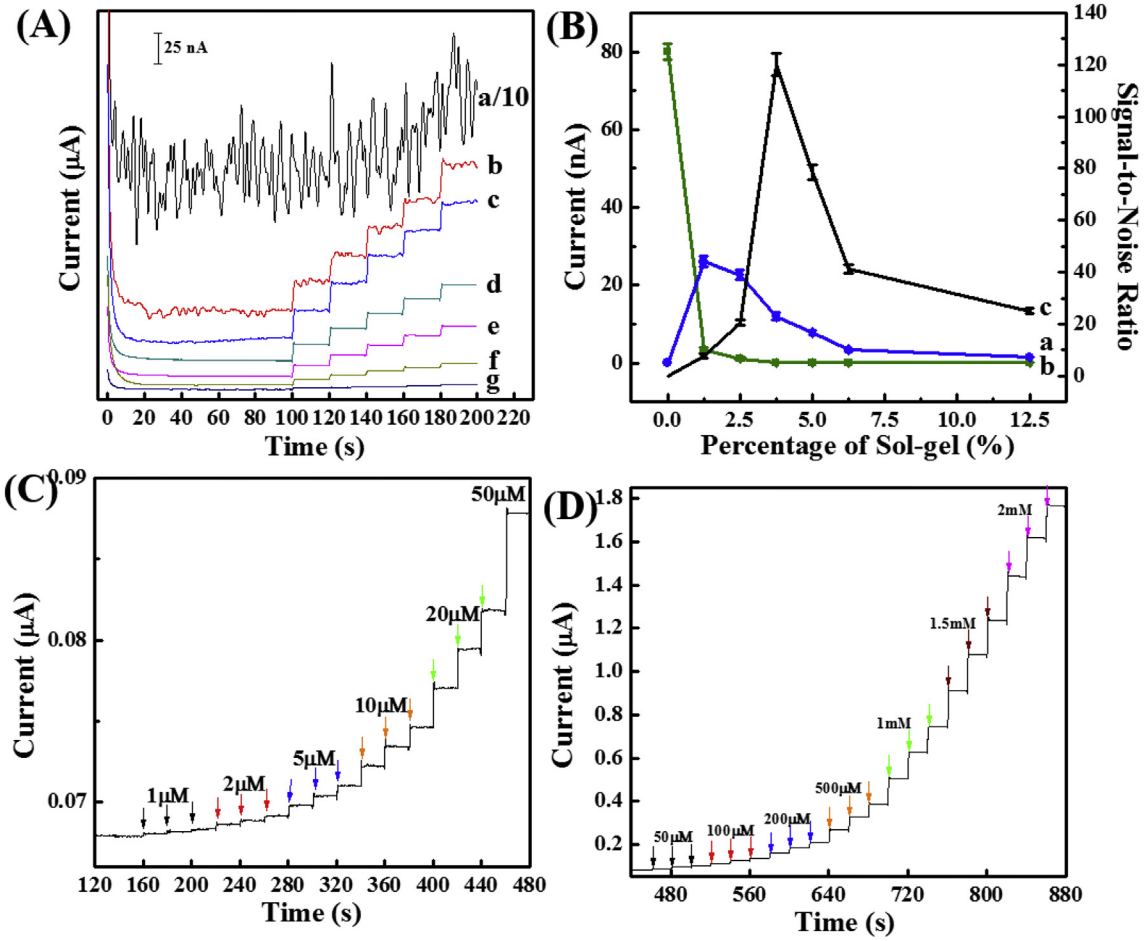

Fig. 3. A) Comparison of amperometric responses obtained from the GC/Au NFs/GS-IL-Au NRs (sol-gel a: 0%; b: 1.25%; c:2.5%; d: 3.75%; e: 5%; f: 6.25%; g: 12.5%) electrodes towards 100 μM H_2O_2, and B) The corresponding a) signal; b) noise; c) signal/noise of the electrodes in A. Attention: considering the noise in GC/Au NFs/GS-IL-Au NRs (sol-gel a: 0%) electrodes, we decrease their signal and noise into 10% here. C), D) Typical amperometric responses obtained by GC/Au NFs/GS-IL-Au NRs (sol-gel 3.75%) electrode with successive addition of specific concentrations of H_2O_2 from 1 μM to 2 mM.

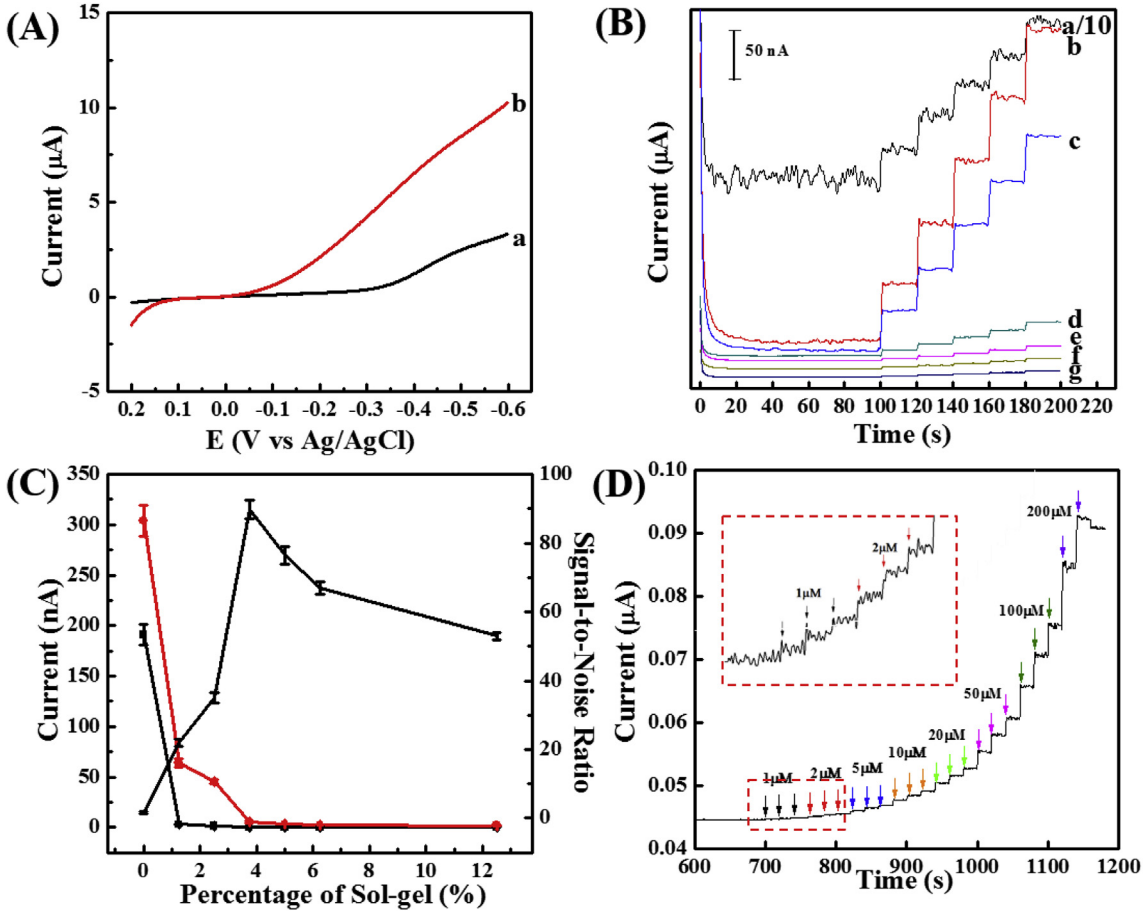

Fig. 4. A) LSV of GC/Au NFs/GS-IL-Au NRs (sol-gel 3.75%)/GOx biosensor toward 5 mM glucose in aCSF (a) without, (b) with 5 mM glucose. B) Comparison of amperometric responses obtained from the GC/Au NFs/GS-IL-Au NRs (sol-gel a: 0%; b: 1.25%; c:2.5%; d: 3.75%; e: 5%; f: 6.25%; g:12.5%)/GOx biosensors towards 100 μM glucose. and C) The corresponding a) signal; b) noise; c) signal/noise of with the increasing sol-gel in A. D) Amperometric responses obtained by GC/Au NFs/GS-IL-Au NRs (sol-gel 3.75%)/GOx biosensor with successive addition of specific concentrations of glucose from 1 μM to 200 μM.

background response and better signal-to-background ratio. And it is of great importance to control the relative contents of the sol-gel when employing this 3D network composite.

Based on the well-balanced signal and noise of the Au NFs/GS-IL-Au NRs (sol-gel 3.75%) film, the typical amperometric responses of this film with successive additions of H_2O_2, which depicted the good relationship between the increment in the reduction current of this electrode and the concentration of H_2O_2. As shown in Fig. 3C and D, the peak currents increased linearly with the concentration of H_2O_2 ranging from 1 μM to 10.164 mM with a slope of 116.85 nA/mM. The detection limit (LOD) was calculated to be 0.28 μM based on 3σ of the background noise.

3.3. Electrochemical behaviour of the 3D network materials modified biosensors towards glucose

In view of the good catalytic performance of the GC/Au NFs/GS-IL-Au NRs (sol-gel 3.75%) electrode towards H_2O_2 above, LSV performances of GC/Au NFs/GS-IL-Au NRs (sol-gel 3.75%)/GOx biosensor in aCSF with (curve b) and without glucose (curve a) were studied (Fig. 4A). The reduction current of this biosensor started to increase at −0.05 V, which can be attributed to the generation of H_2O_2 from the oxidation of glucose. The relative low on-set potential further confirmed the good electrocatalytic property of the optimized Au NFs/GS-IL-Au NRs (sol-gel 3.75%) materials. In an effort to assess the effect of the sol-gel amount on the performance of the glucose biosensor, the amperometric responses of the fabricated biosensors based on series 3D network materials towards the detection of glucose have been carefully recorded by successively adding 100 μM glucose in aCSF solution (Fig. 4B). A remarkably high background noise resulting in a lowest signal/noise value was observed on the GC/Au NFs/GS-IL-Au NRs (sol-gel 0%, curve a)/GOx biosensor. After that, both gradually descending signal reduction currents and background noises were observed on each GC/Au NFs/GS-IL-Au NRs (sol-gel 1.25%, curve b; 2.5%, curve c; 3.75%, curve d; 5%, curve e; 6.25%, curve f; 12.5%, curve g)/GOx biosensors. All the signal/noise values were summarized in Fig. 4C, which were highly coinciding with that of H_2O_2 sensing.

In effort to confirm the contribution of AuNFs in the biosensor's performance, GC/Au NFs/GS-IL-Au NRs (sol-gel 3.75%)/GOx biosensor and GC/GS-IL-Au NRs (sol-gel 3.75%)/GOx biosensor were prepared. Their amperometric responses towards 100 μM glucose were investigated and depicted in Fig. S5. Without the electrodeposition of Au NFs, the GC/GS-IL-Au NRs (sol-gel 3.75%)/GOx biosensor presented dramatically decreased current response towards 100 μM glucose. Moreover, a stable background current was achieved after a relative long period (600 s). This is because the GC/GS-IL-Au NRs (sol-gel 3.75%)/GOx composite is unstable on the electrode and easy to be removed in a stirring solution. Whereas, for GC/Au NFs/GS-IL-Au NRs (sol-gel 3.75%)/GOx biosensor, with higher sensitivity, the stable current was reached within 20 s. With the modified of Au NFs layer, the GS-IL-Au NRs (sol-gel 3.75%) are assembled onto the Au surface by covalent Au−S bonds to form a stable 3D porous structure, which offers a stereo attaching sites for GOx immobilization.

Fig. 4D illustrates the typical amperometric responses of the GC/Au

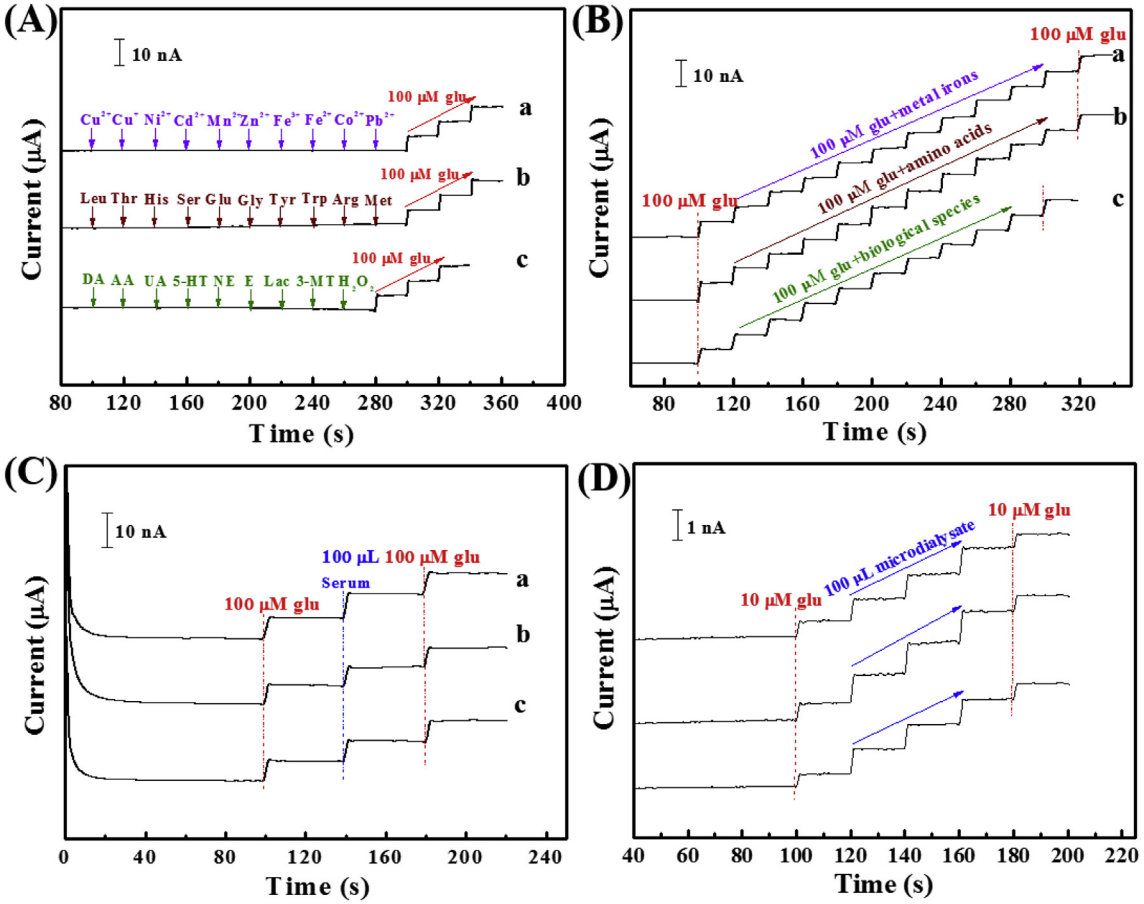

Fig. 5. Amperometric responses of GC/Au NFs/GS-IL-Au NRs (sol-gel 3.75%)/GOx biosensor in aCSF with successive addition of (A) metal ions (Cu^{2+}, Cu^{+}, Ni^{2+}, Cd^{2+}, Mn^{2+}, Zn^{2+}, Fe^{3+}, Fe^{2+}, Co^{2+}, Pb^{2+}, (10 μM, curve a)); amino acids (Leu, Thr, His, Ser, Glu, Gly, Tyr, Trp, Arg, Met, (10 μM, curve b)); biological species (10 μM DA, 100 μM AA, 50 μM UA, 1 μM 5-HT, NE and E, 1 mM Lac, 10 μM 3-MT, 1 μM H_2O_2, (curve c)) and 100 μM glucose; (B) 100 μM glucose containing metal ions (curve a); amino acids (curve b); biological species (curve c); the concentrations are the same with that in (A); (C)100 μM glucose, 100 μL serum and 100 μM glucose, blank PBS: 5 mL; (D) 10 μM glucose, 100 μL microdialysate, 10 μM glucose, blank aCSF: 3 mL.

NFs/GS-IL-Au NRs (sol-gel 3.75%)/GOx biosensor with successive additions of glucose. The peak currents increased linearly with the concentration of glucose ranging from 1 μM to 0.764 mM with a slope of 64.08 nA/mM. The background noise obtained on the GC/Au NFs/GS-IL-Au NRs (sol-gel 3.75%)/GOx biosensor was 0.005 nA, and the LOD was calculated to be 0.38 μM based on 3σ of the background noise. This LOD value is superior to that of previously reported biosensors, which indicates that the present glucose biosensor holds great promising for glucose assay in a biological system [34–42]. A table has been summarized to more clearly compare the proposed 3D network materials based biosensor with other materials based platforms (Table S1). The apparent (K_m^{app}), which is an indication of enzyme–substrate kinetics, can be calculated according to the Lineweaver–Burk equation [43]. In this work, the K_m^{app} value was about 0.302 mM, much smaller than previous relative reports [44,45]. Since the smaller K_m^{app} shows the higher catalytic ability, a clear conclusion can be drawn GC/Au NFs/GS-IL-Au NRs (sol-gel 3.75%)/GOx biosensor displays a higher affinity and enzymatic activity in the range of lower concentration of glucose.

Several advantages of the proposed biosensor contribute to its high sensitivity. First, thiol-containing silica sol-gel provides stereo attaching sites for GS-IL and Au NRs, which can be assembled onto GC/Au NFs electrode to form a 3D network structure. Because of the electrostatic attraction between GS-IL and GOx, enzymes can be firmly immobilized on the electrode. And the good biocompatibility of the 3D network materials and GOx provide a favorable microenvironment for preserving the activity of enzyme. Second, self-assembly of GS-IL-Au NRs to sol-gel provides the benign conduction pathways and enables efficient electron tunneling, which makes it possible to realize fast electron transfer from the enzymes to the electrode surface. And the effective 3D porous structure offers a “transport channel” to facilitate the transport of the substrate and electron.

3.4. Selectivity and stability of the optimized 3D network materials modified biosensors

The complexity of biosystem presents a great challenge to the present biosensor for glucose detection in selectivity. The selectivity of the present method was evaluated by monitoring the response current of the biosensor to sense the potential interferences in the absence/presence of glucose. The possible interferences for glucose detection that commonly coexist in biosystem are metal ions (Cu^{2+}, Cu^{+}, Ni^{2+}, Cd^{2+}, Mn^{2+}, Zn^{2+}, Fe^{3+}, Fe^{2+}, Co^{2+}, Pb^{2+}, amino acids (Leu, Thr, His, Ser, Glu, Gly, Tyr, Trp, Arg, Met); several typical biological species (DA, AA, 5 UA, 5-HT, NE, E, Lac, H_2O_2). Remarkably, as shown in Fig. 5A and B, no obvious responses were observed with additions of these mentioned interferences, and all the potential interferences showed negligible effects on the current signal for glucose sensing. These evidences indicate the high selectivity of the present biosensor for glucose determination against metal ions, amino acids and biological species in the biosystem, which is attributed to the high specificity of GOx.

To further study the antifouling properties of the GC/Au NFs/GS-IL-Au NRs (sol-gel 3.75%)/GOx biosensor against proteins, we performed the electrochemical studies with BSA which is commonly used in antifouling researches. The amperometric responses of the biosensor

toward glucose followed by the addition of BSA into solution were recorded. As shown in Fig. S6, the addition of BSA induced a slight decrease in amperometric current responses, which may be because the protein trapped in the 3D network materials brings mild damage to the electron transfer between enzyme and electrode redox center. Nonetheless, the decrease in current response is tiny, which should not exert significant effect on the glucose determination of real sample with a few protein.

The stability of the GC/Au NFs/GS-IL-Au NRs (sol-gel 3.75%)/GOx biosensor was tested by storing it at 4 °C for 40 days. The biosensor retained almost 79.53% of their initial activity (data not shown). The effective retention of the biosensor can be explained by the combination of several factors. First, the GS-IL, positively charged, provides a favorable environment for better retention of negatively charged GOx. Second, the biocompatibility of GS-IL/Au nanorods with GOx enzyme provides substantial improvement in long-term stability of the glucose biosensor. Third, the sol-gel provides 3D network structure to encapsulate GOx effectively, which may contribute to the prevention of GOx leaching.

3.5. Analysis of glucose in real sample

The GC/Au NFs/GS-IL-Au NRs (sol-gel 3.75%)/GOx biosensor for glucose sensing showed high sensitivity and selectivity, which can be applied in real sample assay. The accuracy of the biosensor was calibrated by glucose standard solutions before and after real sample measurement. Firstly, the serum sample (100 μL) was added into the stirred 5 mL PBS and amperometric response was recorded at −0.2 V (Fig. 5C). The results were shown in Table S2. The glucose levels determined in this study were close to the values measured by spectrophotometric method in hospital, indicating that the fabricated glucose biosensor has practical potential. Furthermore, the present biosensor was used to glucose assay in cerebral microdialysate (Fig. 5D) as above. The basal level of glucose in the microdialysate from the rat striatum (Table S3) are comparable to previously reported works [42,46]. This demonstrates that the proposed biosensor for glucose sensing can satisfy the requirements of complex sample detection and has bright potential in therapeutic diagnostics.

4. Conclusions

In summary, a novel 3D network materials was fabricated by self-assembly of GS-IL and Au NRs into the thiolated sol–gel. The electrochemical performance of the 3D network materials were affected by the Au NRs structure and the doing amount of sol-gel. With the optimized sol-gel content (3.75%) and Au NRs (aspect ratio 2.6), the 3D network materials based glucose biosensor with low background signal revealed high sensitivity and selectivity towards glucose determination. The remarkable analytical performance of the biosensor, enables us for real sample assay including serum and brain microdialysate. Although the construction of the biosensor is complicated, the thiolated sol–gel provides an alternative excellent matrix to reduce the background signals of the high electroactive catalysts, thus contributing to promoted sensitivities. Beyond this, the sol-gel created a favorable 3D environment for nanomaterials modification and enzyme immobilization for use in various biocatalytic and bioelectrocatalytic applications.

Conflicts of interest

There are no conflicts to declare.

Acknowledgements

This work was supported by the National Natural Science Foundation of China (Project No. 21605047), Natural Science Foundation of Hunan Province (Project No. 2017JJ3080), Science and Technology Planning Project of Hunan Province (Project No. 17C0627).

Appendix A. Supplementary data

Supplementary data to this article can be found online at https://doi.org/10.1016/j.ab.2018.12.012.

References

[1] R. Li, D. Guo, J. Ye, M. Zhang, Stabilization of Prussian blue with polyaniline and carbon nanotubes in neutral media for in vivo determination of glucose in rat brains, Analyst 140 (2015) 3746–3752.
[2] R. Chen, W. Xu, C. Xiong, X. Zhou, S. Xiong, Z. Nie, L. Mao, Y. Chen, H.C. Chang, High-salt-tolerance matrix for facile detection of glucose in rat brain microdialysates by MALDI mass spectrometry, Anal. Chem. 84 (2012) 465–469.
[3] H. Gu, Y. Yang, X. Zhou, T. Zhou, G. Shi, Online electrochemical method for continuous and simultaneous monitoring of glucose and l-lactate in vivo with graphene hybrids as the electrocatalyst, J. Electroanal. Chem. 730 (2014) 41–47.
[4] F. Palmisano, R. Rizzi, D. Centonze, P.G. Zambonin, Simultaneous monitoring of glucose and lactate by an interference and cross-talk free dual electrode amperometric biosensor based on electropolymerized thin films, Biosens. Bioelectron. 15 (2000) 531–539.
[5] F.F. Zhang, Q. Wan, C.X. Li, X.L. Wang, Z.Q. Zhu, Y.Z. Xian, L.T. Jin, K. Yamamoto, Simultaneous monitoring of glucose, lactate, L-glutamate and hypoxanthine levels in rat striatum by a flow-injection enzyme electrode array system with in vivo microdialysis sampling, J. Electroanal. Chem. 575 (2005) 1–7.
[6] R.B. Rakhi, P. Nayak, C. Xia, H.N. Alshareef, Novel amperometric glucose biosensor based on MXene nanocomposite, Sci. Rep. 6 (2016) 36422.
[7] H.J. Parab, C. Jung, J.H. Lee, H.G. Park, A gold nanorod-based optical DNA biosensor for the diagnosis of pathogens, Biosens. Bioelectron. 26 (2010) 667–673.
[8] S. Hebié, L. Cornu, T.W. Napporn, J. Rousseau, B.K. Kokoh, Insight on the surface structure effect of free gold nanorods on glucose electrooxidation, J. Phys. Chem. C 117 (2013) 9872–9880.
[9] T. Kuila, S. Bose, P. Khanra, A.K. Mishra, N.H. Kim, J.H. Lee, Recent advances in graphene-based biosensors, Biosens. Bioelectron. 26 (2011) 4637–4648.
[10] K.S. Novoselov, A.K. Geim, S.V. Morozov, D. Jiang, Y. Zhang, S.V. Dubonos, I.V. Grigorieva, A.A. Firsov, Electric field effect in atomically thin carbon films, Science 306 (2004) 666–669.
[11] A. Ambrosi, C.K. Chua, N.M. Latiff, A.H. Loo, C.H.A. Wong, A.Y.S. Eng, A. Bonanni, M. Pumera, Graphene and its electrochemistry – an update, Chem. Soc. Rev. 45 (2016) 2458–2493.
[12] J. Shi, X. Li, Q. Chen, K. Gao, H. Song, S. Guo, Q. Li, M. Fang, W. Liu, H. Liu, X. Wang, A monocrystal graphene domain biosensor array with differential output for real-time monitoring of glucose and normal saline, Nanoscale 7 (2015) 7867–7872.
[13] H. Lee, T.K. Choi, Y.B. Lee, H.R. Cho, R. Ghaffari, L. Wang, H.J. Choi, T.D. Chung, N. Lu, T. Hyeon, S.H. Choi, D.H. Kim, A graphene-based electrochemical device with thermoresponsive microneedles for diabetes monitoring and therapy, Nat. Nanotechnol. 11 (2016) 566–572.
[14] T.T. Baby, S.S.J. Aravind, T. Arockiadoss, R.B. Rakhi, S. Ramaprabhu, Metal decorated graphene nanosheets as immobilization matrix for amperometric glucose biosensor, Sens. Actuators, B 145 (2010) 71–77.
[15] X. Wang, X. Zhang, Electrochemical co-reduction synthesis of graphene/nano-gold composites and its application to electrochemical glucose biosensor, Electrochim. Acta 112 (2013) 774–782.
[16] H.J. Kang, M.A. Aziz, B. Jeon, K. Jo, H. Yang, Strategy for low background-current levels in the electrochemical biosensors using horse-radish peroxidase labels, Electroanalysis 21 (2009) 2647–2652.
[17] Y. Fang, D. Zhang, Y. Guo, Y. Guo, Q. Chen, Simple one-pot preparation of chitosan-reduced graphene oxide-Au nanoparticles hybrids for glucose sensing, Sens. Actuators, B 221 (2015) 265–272.
[18] H. Wu, J. Wang, X. Kang, C. Wang, D. Wang, J. Liu, I.A. Aksay, Y. Lin, Glucose biosensor based on immobilization of glucose oxidase in platinum nanoparticles/graphene/chitosan nanocomposite film, Talanta 80 (2009) 403–406.
[19] P. Rafighi, M. Tavahodi, B. Haghighi, Fabrication of a third-generation glucose biosensor using graphene-polyethyleneimine-gold nanoparticles hybrid, Sens. Actuators, B 232 (2016) 454–461.
[20] S. Palanisamy, R. Devasenathipathy, S.M. Chen, M. Ajmal Ali, C. Karuppiah, V. Balakumar, P. Prakash, M.S. Elshikh, F.M.A. Al-Hemaid, Direct electrochemistry of glucose oxidase at reduced graphene oxide and β-cyclodextrin composite modified electrode and application for glucose biosensing, Electroanalysis 27 (2015) 2412–2420.
[21] R. Gupta, N.K. Chaudhury, Entrapment of biomolecules in sol–gel matrix for applications in biosensors: problems and future prospects, Biosens. Bioelectron. 22 (2007) 2387–2399.
[22] J. Lia, S.N. Tana, H. Ge, Silica sol-gel immobilized amperometric biosensor, Anal. Chim. Acta 335 (1996) 137–145.
[23] B. Wang, B. Li, Q. Deng, S. Dong, Amperometric glucose biosensor based on sol-gel organic-inorganic hybrid material, Anal. Chem. 70 (1998) 3170–3174.
[24] J. Jia, B. Wang, A. Wu, G. Cheng, Z. Li, S. Dong, A method to construct a third-generation horseradish peroxidase biosensor: self-assembling gold nanoparticles to three-dimensional sol-gel network, Anal. Chem. 74 (2002) 2217–2223.
[25] H.H. Chang, C.J. Murphy, Mini gold nanorods with tunable plasmonic peaks beyond

1000 nm, Chem. Mater. 30 (2018) 1427–1435.
[26] H. Gu, Y. Yu, X. Liu, B. Ni, T. Zhou, G. Shi, Layer-by-layer self-assembly of functionalized graphene nanoplates for glucose sensing in vivo integrated with on-line microdialysis system, Biosens. Bioelectron. 32 (2012) 118–126.
[27] K. Krishnamoorthy, M. Veerapandian, R. Mohan, S.J. Kim, Investigation of Raman and photoluminescence studies of reduced graphene oxide sheets, Appl. Phys. A 106 (2011) 501–506.
[28] A.L. Higginbotham, D.V. Kosynkin, A. Sinitskii, Z.Z. Sun, J.M. Tour, Lower-defect graphene oxide nanoribbons from multiwalled carbon nanotubes, ACS Nano 4 (2010) 2059–2069.
[29] L. Zhang, Y. Han, F. Zhao, G. Shi, Y. Tian, A selective and accurate ratiometric electrochemical biosensor for monitoring of Cu^{2+} ions in a rat brain, Anal. Chem. 87 (2015) 2931–2936.
[30] B.R. Shrestha, A. Nishikata, T. Tsuru, Application of channel flow double electrode to the study on gold dissolution during potential cycling in sulfuric acid solution, J. Electroanal. Chem. 665 (2012) 33–37.
[31] D.A.J. Rand, R. Woods, A study of the dissolution of platinum, palladium, rhodium and gold electrodes in 1 m sulphuric acid by cyclic voltammetry, J. Electroanal. Chem. Interfacial Electrochem. 35 (1972) 209–218.
[32] J. Guo, Y. Wang, M. Zhao, 3D flower-like ferrous(II) phosphate nanostructures as peroxidase mimetics for sensitive colorimetric detection of hydrogen peroxide and glucose at nanomolar level, Talanta 182 (2018) 230–240.
[33] F.R. de Souza, G.L. Alves, W.K. Coltro, Capillary-driven toner-based microfluidic devices for clinical diagnostics with colorimetric detection, Anal. Chem. 84 (2012) 9002–9007.
[34] G. Fu, X. Yue, Z. Dai, Glucose biosensor based on covalent immobilization of enzyme in sol-gel composite film combined with Prussian blue/carbon nanotubes hybrid, Biosens. Bioelectron. 26 (2011) 3973–3976.
[35] A. Salimi, R.G. Compton, R. Hallaj, Glucose biosensor prepared by glucose oxidase encapsulated sol-gel and carbon-nanotube-modified basal plane pyrolytic graphite electrode, Anal. Biochem. 333 (2004) 49–56.
[36] K. Zhou, Y. Zhu, X. Yang, C. Li, Electrocatalytic oxidation of glucose by the glucose oxidase immobilized in graphene-au-nafion biocomposite, Electroanalysis 22 (2010) 259–264.
[37] X. Jiang, Y. Wu, X. Mao, X. Cui, L. Zhu, Amperometric glucose biosensor based on integration of glucose oxidase with platinum nanoparticles/ordered mesoporous carbon nanocomposite, Sens. Actuators, B 153 (2011) 158–163.
[38] J. Wu, F. Yin, Sensitive enzymatic glucose biosensor fabricated by electrospinning composite nanofibers and electrodepositing Prussian blue film, J. Electroanal. Chem. 694 (2013) 1–5.
[39] N. Chandra Sekar, S.A. Mousavi Shaegh, S.H. Ng, L. Ge, S.N. Tan, A paper-based amperometric glucose biosensor developed with Prussian blue-modified screen-printed electrodes, Sens. Actuators, B 204 (2014) 414–420.
[40] A. Ahmadalinezhad, A.K.M. Kafi, A. Chen, Glucose biosensing based on the highly efficient immobilization of glucose oxidase on a Prussian blue modified nanostructured Au surface, Electr. Commun. 11 (2009) 2048–2051.
[41] X. Guo, B. Liang, J. Jian, Y. Zhang, X. Ye, Glucose biosensor based on a platinum electrode modified with rhodium nanoparticles and with glucose oxidase immobilized on gold nanoparticles, Microchim. Acta 181 (2014) 519–525.
[42] B. Li, Y. Fan, C. Li, X. Zhao, K. Liu, Y. Lin, Online electrochemical monitoring of glucose in rat brain with acanthosphere-like CuOOH nanospheres-based electrochemical sensor as non-enzymatic and O2-independent detector, Electroanalysis (2018).
[43] R.A. Kamin, G.S. Wilson, Rotating ring-disk enzyme electrode for biocatalysis kinetic studies and characterization of the immobilized enzyme layer, Anal. Chem. 52 (1980) 1198–1205.
[44] K. Yang, G.W. She, H. Wang, X.M. Ou, X.H. Zhang, C.S. Lee, S.T. Lee, ZnO nanotube arrays as biosensors for glucose, J. Phys. Chem. C 113 (2009) 20169–20172.
[45] Y. Liu, A.P.F. Turner, M. Zhao, W.C. Mak, Processable enzyme-hybrid conductive polymer composites for electrochemical biosensing, Biosens. Bioelectron. 100 (2018) 374–381.
[46] Y. Yu, Y. Yang, H. Gu, T. Zhou, G. Shi, Size-tunable Pt nanoparticles assembled on functionalized ordered mesoporous carbon for the simultaneous and on-line detection of glucose and L-lactate in brain microdialysate, Biosens. Bioelectron. 41 (2013) 511–518.